Competing d_{xy} and $s_\pm$ pairing symmetries in superconducting La$_3$Ni$_2$O$_7$: LDA + FLEX calculations

Griffin Heier [,1] Kyungwha Park [,2] and Sergey Y. Savrasov [1]

[1]*Department of Physics, University of California, Davis, California 95616, USA*
[2]*Department of Physics, Virginia Tech, Blacksburg, Virginia 24061, USA*

With recent discoveries of superconductivity in infinite–layer nickelates and in La$_3$Ni$_2$O$_7$ under high pressure, new opportunities appeared that yet another family of high-temperature superconductors based on Ni element may exist in nature, as was previously the case of cuprates and iron-based materials. With their famous strong Coulomb correlations among $3d$ electrons and the proximity to antiferromagnetic instability, these systems represent a challenge for their theoretical description, and most previous studies of superconductivity relied on the solutions of simplified few-orbital model Hamiltonians. Here, on the other hand, we use a recently developed combination of density functional theory with momentum and frequency-resolved self-energies deduced from the so-called fluctuational-exchange–type random phase approximation to study spin fluctuation mediated pairing tendencies in La$_3$Ni$_2$O$_7$ under pressure. This methodology uses first-principles electronic structures of an actual material and is free of tight-binding parametrizations employed in the model Hamiltonian approach. Based on our numerical diagonalization of the BCS gap equation, we show that competing d_{xy} and s$_\pm$-pairing symmetries emerge in superconducting La$_3$Ni$_2$O$_7$ with the corresponding coupling constants becoming large in the proximity of spin-density-wave instability. The results presented here are discussed in light of numerous other calculations and provide ongoing experimental efforts with predictions that will allow further tests of our understanding of unconventional superconductors.

I. INTRODUCTION

Opportunities to realize high-temperature superconductivity have always been a subject of enormous research interest, and recent discoveries of superconducting nickelates [1,2] are not an exception. Despite numerous theoretical and experimental efforts in the past [3–8], infinite-layer Nd$_2$NiO$_2$ was shown to exhibit superconductivity at 8 K only a few years ago [1,9–11], but just-discovered 80 K superconductivity in bulk La$_3$Ni$_2$O$_7$ under applied pressure over 14 GPa [2] has brought nickelates into focus of becoming an addition to the famous family of high-temperature superconducting cuprates and ironates [12–14].

This breakthrough has inspired a large-scale theoretical effort to understand the nature of superconductivity in La$_3$Ni$_2$O$_7$. First-principles electronic-structure calculations based on density functional theory (DFT) and local density approximation (LDA) [15] reveal the dominant role of Ni $3d_{x^2-y^2}$ orbitals and, in addition, of Ni $3d_{3z^2-r^2}$ orbitals [2,16,17]. Correlation effects beyond DFT have been studied [18–20] using combinations of LDA and GW methods with dynamical mean field theory (LDA + DMFT and GW + DMFT) [21]. A two–orbital bilayer model for the bands near the Fermi level has been proposed to describe the low-energy physics of this material [22,23]. Many-body simulations of model Hamiltonians with quantum Monte Carlo [24] and density matrix renormalization group [25] techniques have also recently appeared.

Focusing on the superconducting state, the discussion of the pairing symmetry has been the subject of extensive studies

in a series of recent works [20,26–32]. Within the two-orbital tight-binding model, the pairing instability was studied using the functional renormalization group (FRG) approach and the multiorbital $t - J$ model. An s$_\pm$-wave pairing with sign-reversal gaps on different Fermi surfaces is revealed, reminiscent of iron-based superconductors [26]. Employing the static auxiliary field Monte Carlo approach to simulate a minimal effective model containing local $d_{3z^2-r^2}$ interlayer spin singlets and metallic $d_{x^2-y^2}$ bands, the authors of Ref. [27] reached a similar conclusion, together with other FRG calculations that also yielded s$_\pm$-wave Cooper pairing triggered by the spin fluctuations [28]. The cellular version of the DMFT was used on the two-orbital Hubbard model where s$_\pm$ superconductivity was observed [29].

Several calculations of the pairing interaction have been performed [20,30–32] using the two-orbital model and the random phase approximation (RPA)—the method used to understand properties of heavy fermion systems many years ago [33,34]. Diagrammatically, the RPA includes particle-hole ladder and bubble diagrams [35,36]. The inclusion to these series of particle-particle ladder diagrams has also been proposed in the past, which was entitled as the Fluctuational Exchange Approximation (FLEX) [37]. This contribution was however found to be not essential in the proximity to magnetic instability where the most divergent terms are described by the particle–hole ladders [38].

Using the RPA, the intraorbital Coulomb interaction parameter $U = 0.8\,\mathrm{eV}$, $J = U/4$, and the interorbital repulsion $V = U - 2J$, the pairing instability was shown to be induced in the s$_\pm$-wave channel due to nesting between the

$(1/2, 1/2)2\pi/a$ and $(1/2, 0)2\pi/a$ points in the Brillouin zone (BZ) [30]. A different RPA calculation [20] discussed the appearance of multiple leading symmetries ($d_{x^2-y^2}$ vs d_{xy}) in the calculation with $U = 0.36$ eV and by utilizing either $J = U/4$ or $U/7$, while the solution of the s$_\pm$ symmetry was found as the subleading one. The study of the paring symmetry as a function of U and using the Kanamori rule $J = U/4$, $V = U - 2J$ has been performed in Ref. [31], where it was shown that s$_\pm$ slightly dominates over d_{xy} symmetry once the system is tuned to the spin-density wave (SDW) instability occurring for the two-orbital model at U slightly above 1.2 eV. A recent work [32] utilized maximally localized Wannier-function construction and found that the superconducting symmetry of La$_3$Ni$_2$O$_7$ is robustly d_{xy} if its LDA band structure is accurately reproduced in the downfolded model.

We have recently implemented a combination of density-functional electronic structure theory with momentum—and energy-dependent self–energy deduced from the above-mentioned FLEX–RPA approach [39]. Such a method is free of tight-binding parametrizations and utilizes full electronic energy bands and the wave functions available in the density-functional calculation. It evaluates dynamical charge and spin susceptibilities of the electrons in a Hilbert space restricted by correlated orbitals only, similar to popular LDA + U [40] and LDA + DMFT approaches [21]. Evaluations of super-conducting pairing interactions describing scattering of the Cooper pairs at the Fermi surface in a realistic material framework became possible using this method. Our most recent calculations of HgBa$_2$CuO$_4$ [41], a prototype single-layer cuprate superconductor, where a much celebrated $d_{x^2-y^2}$ symmetry of the order parameter was easily recovered with LDA + FLEX, has demonstrated the applicability of this method to study spin-fluctuation mediated superconductivity without reliance on tight-binding approximations of their electronic structures.

Here we apply the LDA + FLEX method to study the superconductivity in bulk La$_3$Ni$_2$O$_7$ under pressure. Our numerically evaluated superconducting pairing interaction de-scribing scattering of the Cooper pairs at the Fermi surface is used to exactly diagonalize the linearized Bardeen-Cooper-Schrieffer (BCS) gap equation on a three-dimensional k-grid of points in the BZ. The highest eigenstate λ_{max} deduced from this procedure represents a spin fluctuational coupling constant similar to the electron–phonon λ_{e-p} in conventional theory of superconductivity. The spin fluctuational λ_{max} was found to be very sensitive to the actual values of the Hubbard interaction U among Ni 3d electrons serving as input to this calculation but reaches rather large values in close proximity to the spin density wave (SDW) instability. This is in accord with a recent RPA study of this system using the tight-binding simulation [31].

The same sensitivity to input U is seen in our calculated normal-state self-energies, which were found to show a weak $\mathbf{k}-$ and strong frequency dependence with particularly large electronic mass renormalization $m^*/m_{LDA} = 1 + \lambda_{sf}$ in the proximity to SDW. Both λ_{max} and λ_{sf} determine the renormalized coupling constant $\lambda_{eff} = \lambda_{max}/(1 + \lambda_{sf})$ that enters the BCS expression for $T_c \approx \omega_{sf} \exp(-1/\lambda_{eff})$, where ω_{sf} is the characteristic energy of spin fluctuations. We find λ_{eff} to be modest and incapable of delivering high critical temperatures

unless we tune U to be very close to the SDW point. Two competing symmetries of the superconducting order parameter, d_{xy} vs s$_\pm$, are seen from the analysis of the highest eigenstates of the BCS gap equation. This result is also found in our own and published [20,30–32] tight-binding RPA simulations. The realization of d_{xy} would be quite unusual in light of the $d_{x^2-y^2}$ pairing state being found in cuprates [42] and of s$_\pm$ pairing in ironates. Due to the appearance of nodes in d_{xy} and its absence in s$_\pm$ symmetry, the ongoing experimental efforts should easily elucidate which pairing symmetry is realized here.

Our paper is organized as follows: In Sec. II, we discuss the results of the correlated electronic structure for La$_3$Ni$_2$O$_7$ using the LDA + FLEX formalism. In Sec. III, we present our results of exact diagonalization of the linearized BCS equation and correspondingly extracted superconducting energy gaps and the eigenvalues as a function of U. We also give estimates of the spin fluctuational mass enhancement that determines the effective coupling constant λ_{eff} entering the BCS expression for the T_c. In Sec. IV, we repeat the calculation using the two-orbital bilayer tight-binding model and give comparisons with our full LDA + FLEX calculation. Section V is the conclusion.

II. ELECTRONIC STRUCTURE OF La$_3$Ni$_2$O$_7$ FROM LDA + FLEX

A unit cell of bulk La$_3$Ni$_2$O$_7$ contains two Ni–O planes and is expected to have its orthorhombic structure with space group $Fmmm$ [43]. This is also true under applied pressure [2]. At 30 GPa, the theoretically deduced lattice parameters are given by $a = 5.29$ Å, $b = 5.21$ Å, $c = 19.73$ Å. We perform our density-functional electronic-structure calculations [15] using the full potential linear muffin-tin orbital method [44]. The self–energies for Ni 3d electrons, $\Sigma(\mathbf{k}, \omega)$, are evaluated on the 12 x 12 x 12 grid of $\mathbf{k}$ points and at the frequency range between -13.6 eV and $+13.6$ eV from the Fermi energy based on RPA-FLEX procedure described previously [39,41]. We use the values of an on–site Hubbard interaction $U = 3$ eV and $J = 0.5$ eV as an input to the simulation similarly to Ref. [22].

Since the self-energy has both real and imaginary parts, the electronic states no longer have infinite life times. We evaluate the poles of the single-particle Green's function, and the obtained Im$G(\mathbf{k}, \omega)$ for La$_3$Ni$_2$O$_7$ is shown in Fig. 1. The Fermi surface states mainly consist of Ni-3$d_{x^2-y^2}$ and Ni-3$d_{3z^2-r^2}$ orbital character. There is a small La-based pocket around the Γ point whose exact position depends on whether one uses theoretical (as in some previous works [22]) or experimental atomic positions utilized here. Such sensitivity was investigated in detail in Ref. [18], but, in any case, it should be irrelevant for the superconducting behavior of La$_3$Ni$_2$O$_7$.

Most of the poles are seen as sharp resonances (plotted in black) in the function Im$G(\mathbf{k}, \omega)$ that closely follows the LDA energy dispersions (plotted in red). However, the difference is seen in the behavior of the Ni 3$d_{x^2-y^2}$ and Ni-3$d_{3z^2-r^2}$ states in the vicinity of the Fermi surface that acquire a strong damping at energies away from the Fermi level. As the primary effect of the self–energy is the renormalization of the electronic
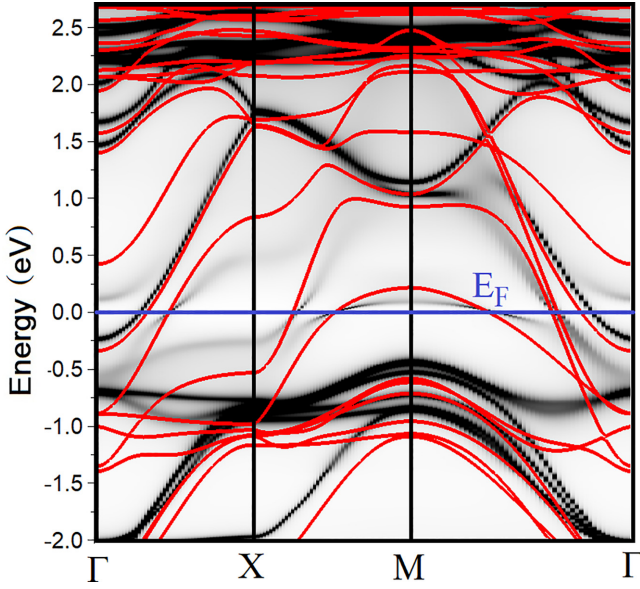
FIG. 1. Electronic structure of $La_3Ni_2O_7$ with experimentally determined lattice parameters that correspond to pressure 30 GPa calculated using LDA + FLEX method (gray shading) with $U = 3$ eV and $J = 0.5$ eV, as well as the result of the density functional LDA calculation (red lines).

bandwidth, we found the electronic mass enhancement to be around 3.4 for Ni $3d_{x^2-y^2}$ and 4.7 for Ni $3d_{3z^2-r^2}$ orbitals using the setup with $U = 3$ eV and $J = 0.5$ eV, but it also needs to be noted that the mass enhancement depends strongly on U, as we discuss later in this paper.

We further plot the diagonal elements of the real and imaginary parts of the self-energy for Ni $3d_{x^2-y^2}$ orbital in Fig. 2. To illustrate the **k** dependence, we show the result for the two points of the BZ: $\Gamma = (0, 0, 0)$ (blue) and $M = (1/2, 1/2, 0)$ (red). We generally find the k dependence of $\Sigma(\mathbf{k}, \omega)$ to be quite small prompting the locality feature of the self-energy. Very similar behavior is seen for other **k** points of the BZ and also for the matrix elements corresponding to $Ni_{d_{3z^2-r^2}}$ orbitals. The local self-energy $\Sigma_{loc}(\omega)$ can be evaluated as an integral over all **k** points, and its frequency dependence is shown in Fig. 2 by small circles. We conclude that there is close agreement between $\Sigma_{loc}(\omega)$ and $\Sigma(\mathbf{k}, \omega)$.

A polelike behavior for the self-energy at frequencies around 2 eV is also seen in our LDA + FLEX calculation. Those poles are led to additional resonances in the single-particle Green's functions that cannot be obtained using static mean DFT-based approaches. The imaginary part of the self-energy nearly diverges indicating strongly damped excitations. Those resonances are usually hard to associate with actual energy bands.

III. SUPERCONDUCTING PROPERTIES OF $La_3Ni_2O_7$ FROM LDA + FLEX

We utilize our LDA + FLEX(RPA) method to evaluate the spin fluctuation mediated pairing interaction. The Fermi surface is triangularized onto small areas described by about 6000 Fermi surface momenta for which the matrix elements
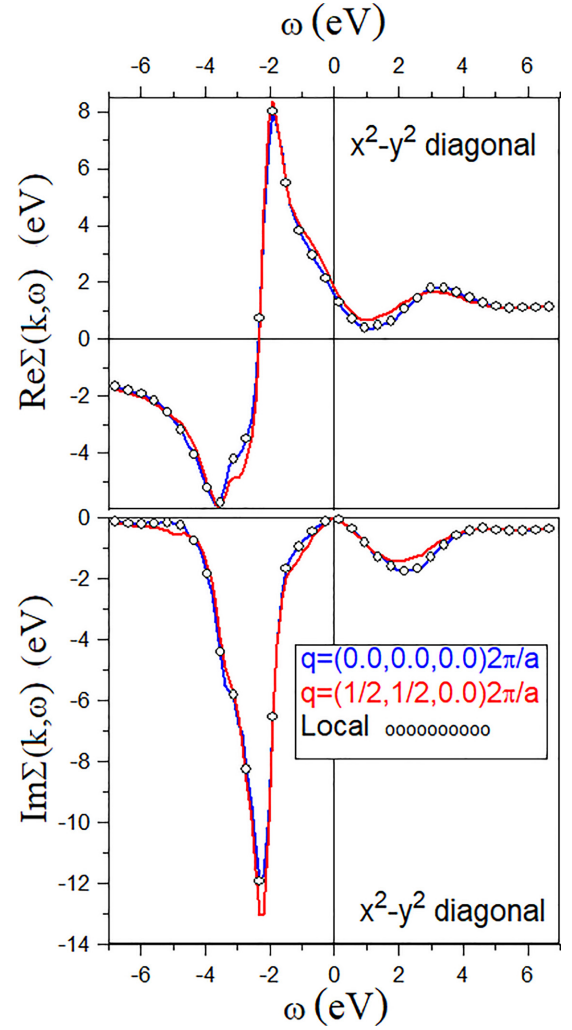

FIG. 2. Calculated self–energy $\Sigma(\mathbf{k}, \omega)$ (top is the real part and bottom is imaginary part) using FLEX-RPA approximation for $d_{x^2-y^2}$ electrons of Ni in $La_3Ni_2O_7$. The wave vectors k correspond to (000) and $(\frac{1}{2}, \frac{1}{2}, 0)$ of the Brillouin zone. The circles show the result of the local self–energy approximation taken as the average over all k points. A representative value of Hubbard $U = 3$ eV and $J = 0.5$ eV is used.

of scattering between the Cooper pairs are calculated using the approach described in Ref. [41]. The linearized BCS gap equation is then exactly diagonalized and the set of eigenstates is obtained for both singlet ($S = 0$) and triplet ($S = 1$) Cooper pairs. The highest eigenvalue λ_{max} represents the physical solution and the eigenvector corresponds to superconducting energy gap $\Delta_S(\mathbf{k}j)$ where **k** is the Fermi surface momentum and j numerates the Fermi surface sheets.

During the course of the diagonalization we, however, find that there are two highest eigenvalues that appear very close to each other. We analyze the behavior of $\Delta_S(\mathbf{k}j)$ corresponding to them as a function of the Fermi momentum using the values of $U = 3$ eV and $J = 0.5$ eV. They are both related to the spin singlet states, and Figs. 3(a) and 3(b) show the first- and second-highest eigenstates, respectively. One can see that the most favorable eigenstate $\Delta_{S=0}(\mathbf{k}j)$ shows the behavior of a d wave with xy symmetry (zeros pointing along k_x and
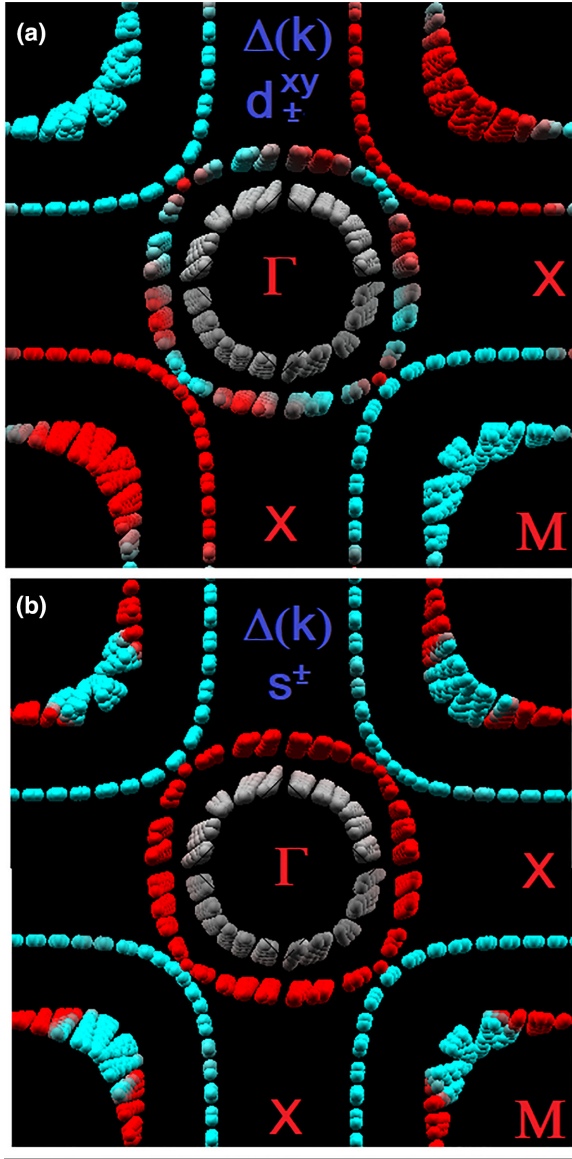
FIG. 3. Calculated superconducting energy gap $\Delta(\mathbf{k})$ for singlet pairing in La$_3$Ni$_2$O$_7$ using numerical solution of the linearized BCS gap equation with the pairing interaction evaluated using LDA + FLEX(RPA) approach. Blue and red color marks point to the quasi-2D Fermi surface (viewed from the top) that corresponds to the negative and positive values of $\Delta(\mathbf{k})$, while the values around zero are colored in gray. Case (a) is the eigenstate with d_{xy} symmetry and (b) is the eigenstate with s$_\pm$ symmetry.

FIG. 4. Calculated using LDA + FLEX(RPA) method dependence of spin fluctuational mass enhancement, λ_{sf}, and the two highest eigenvalues λ_{max} (squares and circles) corresponding to d_{xy} and s$_\pm$ symmetries of the linearized BCS equation as a function of the on-site Hubbard interaction U for d electrons of Ni in La$_3$Ni$_2$O$_7$. The effective coupling constant $\lambda_{eff} = \lambda_{max}/(1 + \lambda_{sf})$ is shown on the right scale.

k_y directions) The plot distinguishes negative and positive values of Δ by blue and red colors while zeros of the gap function are colored in grey as, for example, the case of the La pocket seen around Γ point. This result is interesting because it differs from the predicted behavior in cuprates with their $d_{x^2-y^2}$ symmetry and also from iron pnictides with their s$_\pm$ behavior. As emphasized earlier [30], the Fermi surface nesting here is quite strong for both BZ edges at $(1/2, 0, 0)2\pi/a$ and $(1/2, 1/2, 0)2\pi/a$, which results in a delicate competition between the two SDW instabilities.

Figure 3(b) shows the behavior of the second-highest eigenstate. Here we clearly resolve sign-changing energy gap
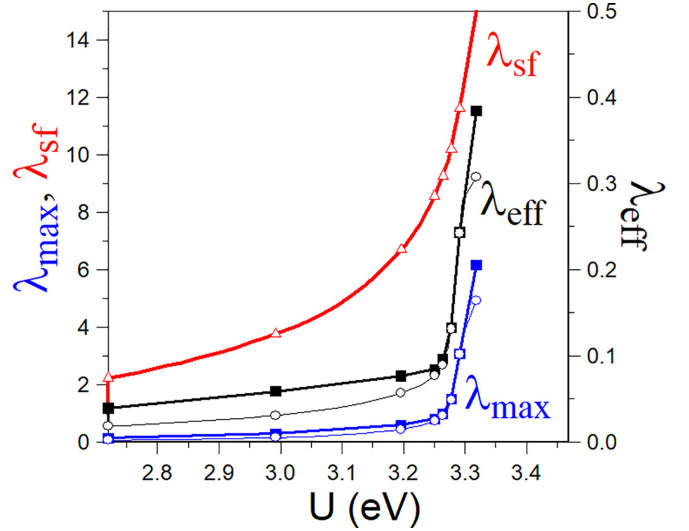
values for different sheets of the Fermi surface corresponding to the s$_\pm$ symmetry. This behavior was recently discussed in several model calculations [26–29]. It was also found explicitly using RPA calculations with the two-orbital bilayer model [30,31].

Several works have emphasized the sensitivity of the solution to both the input interaction parameters U [31], J [20], and the longer range hopping integrals [32], resulting in the appearance of the competing symmetries, such as s$_\pm$, d_{xy} as well as $d_{x^2-y^2}$. Since we use full LDA-derived band structures in the simulation, we can gain additional insight by varying the parameter U. We use its range of values between 2.8 and 3.3 eV and extract from the BCS gap equation the highest eigenstates and their symmetries as a function of U. This plot is shown in Fig. 4, where one can see the dependence of the highest (squares) and the next-highest (circles) eigenvalues as a function of U. We find that d_{xy} symmetry dominates slightly in the range of U's below 3.2 eV but competes closely with the s$_\pm$ symmetry once we approach the SDW instability that occurs above 3.2 eV. Lacking a rigorous procedure for determining U, it is clear that the leading paring symmetry in La$_3$Ni$_2$O$_7$ cannot be exactly predicted using this method and the question should be settled by the experiment.

To get estimates of the critical temperature, we recall that it is not the eigenvalue λ_{max} but an effective coupling constant λ_{eff} that enters the BCS T_c expression: $T_c \approx \omega_{sf} \exp(-1/\lambda_{eff})$. It incorporates the effects associated with the mass renormalization describing the parameter λ_{sf}, and is also weakened slightly by the Coulomb pseudopotential μ_m^*, which should refer to the same pairing symmetry m as λ_{max}:

$$\lambda_{eff} = \frac{\lambda_{max} - \mu_m^*}{1 + \lambda_{sf}}. \tag{1}$$

The mass enhancement can be evaluated as the Fermi surface (FS) average of the electronic self-energy derivative taken at the Fermi level:

$$\lambda_{\mathrm{sf}} = -\left\langle \left. \frac{\partial \Sigma(\mathbf{k}, \omega)}{\partial \omega} \right|_{\omega=0} \right\rangle_{\mathrm{FS}}. \qquad (2)$$

We calculate the dependence of λ_{sf} on U using analytical differentiation of the self-energy at zero frequency by utilizing its spectral representation [45]. λ_{sf} is found to grow rapidly in the vicinity of SDW, as we illustrate in Fig. 4.

To give estimates for the effective coupling constant, λ_{eff}, we notice that μ_m^* is expected to be very small for the pairing symmetries different from the standard s wave [46]. We therefore set this parameter to zero. The plot of $\lambda_{\mathrm{eff}} = \lambda_{\max}/(1 + \lambda_{\mathrm{sf}})$ vs U is shown in Fig. 4, with its scale given on the right. One can see that the range of these values is quite modest (≈ 0.1) for U's less than 3.2 eV as compared to both $\lambda_{\max}$ and λ_{sf}, primarily due to the fact that the rise in the eigenvalue of the gap equation is compensated by the renormalization effect of the electronic self-energy.

Only in close proximity to the SDW instability, λ_{eff} raises to the values ≈ 0.4. (It can go even further up upon tuning U.) However, this corresponds to very large values of $\lambda_{\mathrm{sf}} \approx 15$, which are likely not very realistic. Although experimental determination of the electronic mass enhancement for La$_3$Ni$_2$O$_7$ is not presently available, one can quote a corresponding range of values for high-T_c cuprates: ARPES studies of Bi$_2$Sr$_2$CaCu$_2$O$_{8+\delta}$ produced $0.5 \lesssim \lambda_{\mathrm{sf}} \lesssim 1.7$ [47]. A different work [48] for Bi$_2$Sr$_2$CaCu$_2$O$_8$ and also for La$_{2-x}$Ba$_x$CuO$_4$ reported the estimate $1 \lesssim \lambda_{\mathrm{sf}} \lesssim 2$. Somewhat larger values of the self-energy slope, $4 - 8$, taken for several Fermi momenta have been seen in ARPES analysis of Bi$_{1.74}$Pb$_{0.38}$Sr$_{1.88}$CuO$_{6+\delta}$ [49]. The value of 2.7 along the nodal line was quoted for YBa$_2$Cu$_3$O$_{6.6}$ [50]. Quantum oscillations reported m^* range from 1.9 to 5 (in units of the free electron mass) for various cuprates, including the value of 2.45 ± 0.15 for HgBa$_2$CuO$_{4+\delta}$ [51].

To get estimates for the range of spin fluctuational energies ω_{sf}, we analyze the behavior of the spin susceptibility that is responsible for the spin fluctuational pairing. Since the BCS approximation assumes that the superconducting pairing K operates for the electrons residing at the Fermi surface only, it can be considered as the static ($\omega = 0$) value for the dynamically resolved interaction: $K(\mathbf{q}, \omega) = I + I\chi(\mathbf{q}, \omega)I$. Here I is the static on-site bare interaction matrix that incorporates U and J while $\chi(\mathbf{q}, \omega)$ is the interacting susceptibility matrix. As a result of the Kramers-Kroenig transformation, $\mathrm{Re}K(\mathbf{q}, 0)$ can be expressed via the inverse frequency moment of its imaginary part, $\mathrm{Im}K(\mathbf{q}, \omega)/\omega$, that is further proportional to the imaginary part of the spin susceptibility weighted by ω^{-1}. Thus, the frequency resolution of the spin fluctuational spectrum can be easily analyzed by plotting the function $\mathrm{Im}\chi(\mathbf{q}, \omega)/\omega$. We present this data in Fig. 5. The spin susceptibility is the matrix which has four orbitals corresponding to various d-electron states and also two sites corresponding to two NiO$_2$ planes within the unit cell. We plot the data as a function of frequency for several wave vectors $\mathbf{q}$ traversing along Γ-M line of the BZ and for the largest diagonal elements of the spin susceptibility that we find for Ni $d_{3z^2-r^2}$ orbitals. The spin fluctuational spectrum is primarily
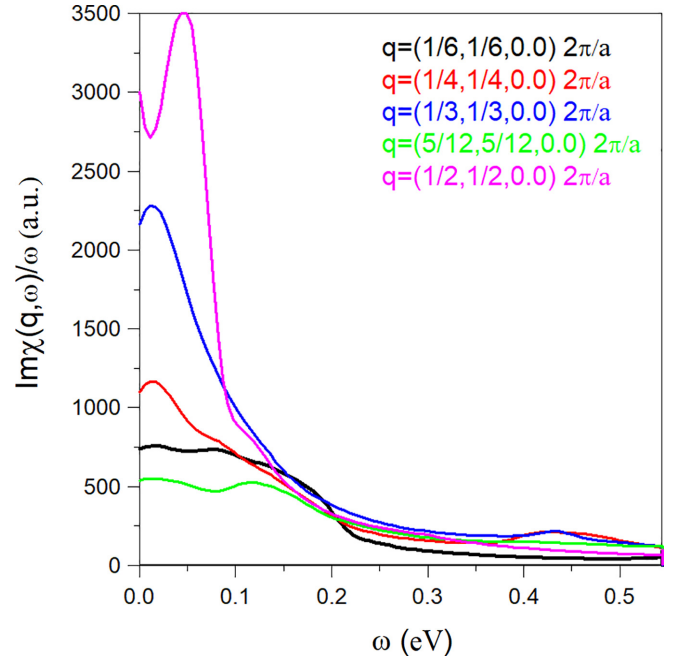

FIG. 5. Calculated imaginary part of spin susceptibility weighted by ω^{-1} in La$_3$Ni$_2$O$_7$ plotted as a function of frequency for several wave vectors q traversing from the Γ to M point of the BZ and for the Ni $d_{3z^2-r^2}$ diagonal elements of the spin susceptibility.

located at small frequencies and peaked around the energies $0.05 eV$ or so. It exhibits significant momentum dependence for Ni $d_{3z^2-r^2}$ orbitals, which shows a broad peak around the momenta $(1/3, 1/3, 0)2\pi/a$ but grows toward the edge of the BZ at $(1/2, 1/2, 0)2\pi/a$. Another maximum was also found around the BZ point $(1/2, 0, 0)2\pi/a$. This indicates that the spin fluctuations are primarily of antiferromagnetic character. Despite long-range antiferromagnetic order being absent in La$_3$Ni$_2$O$_7$, this result is quite similar to cuprates and iron-based materials where doping is served to suppress the long-range magnetic order.

It is interesting to note that the range of $\omega_{\mathrm{sf}} \approx 50$ meV is also seen for high-T_c cuprates as peaks in imaginary spin susceptibility accessible via the neutron scattering experiment [52]. There is a famous 40 meV resonance which is visible in the superconducting state [53]. There are numerous angle-resolved photoemission experiments (ARPES) that show kinks in the one-electron spectra at the same energy range [54]. These kinks are sometimes interpreted as caused by the electron–phonon interactions [55] but, unfortunately, the calculated values of λ_{e-p} are known to be small in the cuprates [56,57]. Note also that for the undoped antiferromagnetic cuprates, the spin wave spectra reside in the energy range of 300 meV [58].

We can judge the values of T_c using our estimated $\omega_{\mathrm{sf}} \approx 50$ meV and the values of λ_{eff} that we calculate in Fig. 4. For $\lambda_{\mathrm{eff}} = 0.1$, the BCS $T_c = \omega_{\mathrm{sf}} \exp(-1/\lambda_{\mathrm{eff}}) \approx 0.02$K. Once we get closer to the SDW instability, the effective coupling increases to the values 0.4 and the corresponding BCS $T_c \approx 48$ K. Given the exponential sensitivity of the T_c, the latter value is certainly not far away from 80 K range.
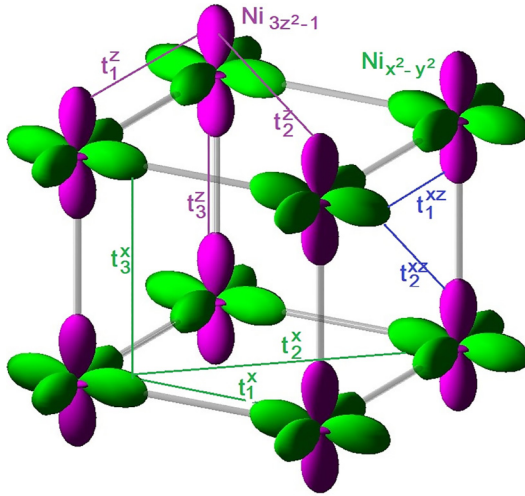
FIG. 6. Two-orbital ($x^2 - y^2$ and $3z^2 - r^2$) bilayer tight-binding model employed for calculations of superconductivity in $La_3Ni_2O_7$.

FIG. 7. Correlation effect using FLEX(RPA) method (black) on the electronic structure of two-orbital bilayer tight–binding model (red) for $La_3Ni_2O_7$.

IV. TIGHT-BINDING CALCULATIONS FOR $La_3Ni_2O_7$

Several tight-binding calculations addressed the origin of superconductivity in $La_3Ni_2O_7$ and the symmetry of the pairing state in recent literature [20,26–32]. Although a few publications predicted $s_\pm$ as leading pairing symmetry [26–30], results based on diagonalizing the BCS gap equation have also emphasized the appearance of the d_{xy} pairing state [20,31,32].

To validate these findings, we have performed our own tight-binding simulations using the FLEX(RPA) method by utilizing the two-orbital (Ni-$d_{x^2-y^2}$ and Ni-$d_{3z^2-r^2}$) model that was proposed to describe the electronic structure of $La_3Ni_2O_7$ [22]. We illustrate this model in Fig. 6, whose parameters are almost identical to those found in Ref. [22]: Using shortcut notations x/z for Ni-$3d_{x^2-y^2}$ and Ni-$3d_{3z^2-r^2}$ orbitals, respectively, we have the on-site energy levels $\epsilon_x = 0.776$ eV, $\epsilon_z = 0.409$ eV, and the hopping integrals as follows: $t_1^x = -0.483$ eV, $t_2^x = 0.069$ eV, $t_3^x = 0.005$ eV, $t_1^z = -0.11$ eV, $t_2^z = -0.017$ eV, $t_3^z = -0.335$ eV, $t_1^{xz} = 0.239$ eV, $t_2^{xz} = -0.034$ eV. (The only difference here is the parameter t_3^z which was quoted to be -0.635 eV in Ref. [22]).

Our tight-binding energy bands are illustrated in Fig. 7 by red lines along the same high–symmetry lines as used in Fig. 1: We conclude that the fit bears close resemblance to the LDA-derived electronic structure.

We further include the effect of Coulomb correlations using the FLEX(RPA) method by calculating the self-energies and single-particle Green's functions. We use the Coulomb interaction parameters as in Ref. [31]: the intraorbital U is fixed to be 1.16 eV, and the exchange integral J is set to $U/4$ while the interorbital Coulomb integral $V = U - 2J$. These parameters are smaller than the ones employed in full LDA + FLEX calculations primarily due to the restricted Hilbert space at which the tight–binding parametrization operates.

The result is illustrated in Fig. 7, where we plot the poles of the Green's function whose frequency dependence is shown by a varied gray shading. In accord with the Fermi liquid
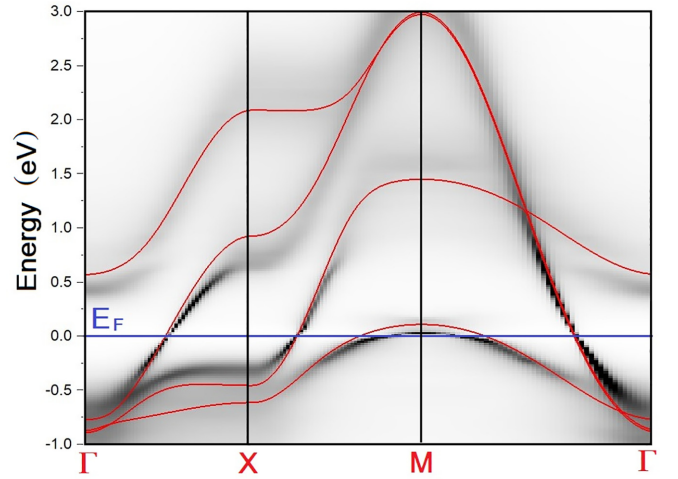
theory, one can see that the long-lived quasiparticles (sharp black lines) are present in the vicinity of the Fermi energy only, while the resonances become more diffusive as we depart from the Fermi level. This is very similar to what we see in our full LDA + FLEX calculations for the bands of predominantly Ni-$d_{x^2-y^2}$ and Ni-$d_{3z^2-r^2}$ character, Fig. 1. There is a small self-energy correction seen for the band around the M point, which would result in a smaller hole pocket predicted by the RPA as compared to the tight-binding fit of the LDA-derived band structure, but since we are not doing self-consistent calculations with respect to the self–energy, the shape of the Fermi surface is fixed to the tight-binding fit while calculating the superconducting pairing interaction.

We further repeat the exact diagonalization of the BCS gap equation using the RPA pairing interaction calculated within the two-orbital bilayer model. The behavior of $\Delta_S(\mathbf{k}j)$ for the two highest eigenvalues is illustrated in Fig. 8, where the plot Fig. 8(a) shows the behavior characteristic for the d_{xy} symmetry while the Fig. 8(b) shows the gap function of the $s_\pm$ symmetry. One can see that momentum dependence of both gap functions is very similar to the ones that we calculate using full LDA + FLEX method; Fig. 3.

It is, however, interesting to note that in the case of the tight–binding calculation, the solution of the $s_\pm$ symmetry always comes out slightly more favorable than the solution of the d_{xy} symmetry. We illustrate this result by plotting the eigenvalue λ_{max} as a function of the parameter U on Fig. 9, where the highest eigenstate marked by squares corresponds to the $s_\pm$ symmetry while the next highest marked by circles is of the d_{xy} symmetry.

Our tight-binding FLEX(RPA) calculation is found in complete agreement with a similar calculation that has recently appeared in the literature [31]. However, it is somewhat different from our LDA + FLEX calculation, where we found that d_{xy} symmetry is more favorable for the range of U's less than 3.2 eV. It is clear that the inclusion of the full LDA energy bands and the wave functions can be a possible source of this discrepancy.
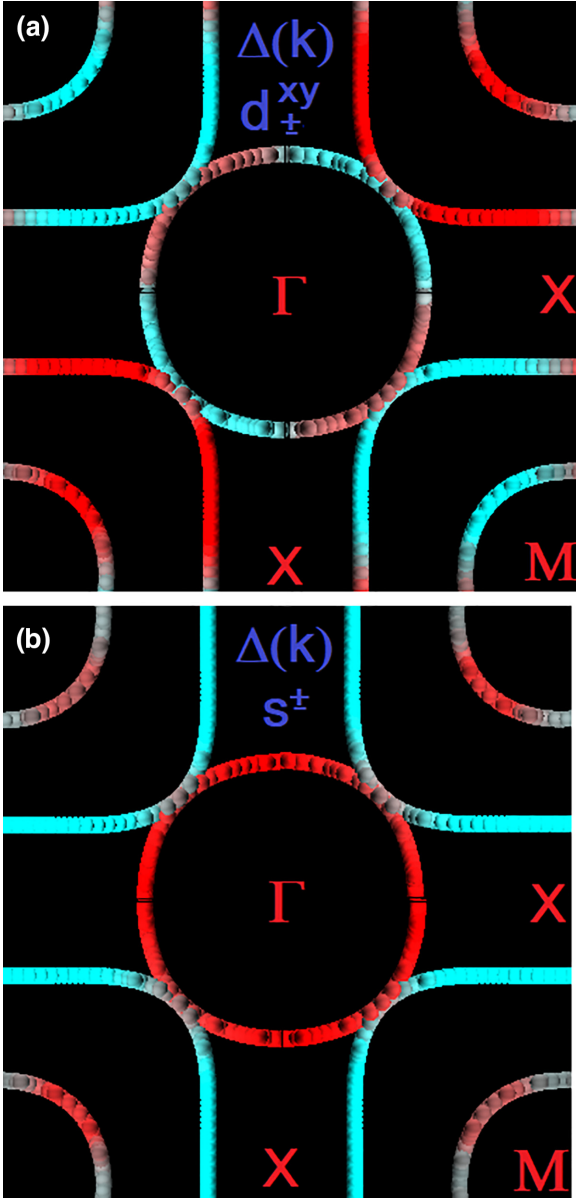
FIG. 8. Calculated superconducting energy gap $\Delta(\mathbf{k})$ for singlet pairing in $La_3Ni_2O_7$ using numerical solution of the linearized BCS gap equation with the pairing interaction evaluated using tight-binding parametrization of the LDA energy bands and FLEX(RPA) method. Blue and red colors mark points at the two–dimensional Fermi surface (viewed from the top) that corresponds to the negative and positive values of $\Delta(\mathbf{k})$, while the values around zero are colored in gray. *a) is the eigenstate with d_{xy} symmetry and (b) is the eigenstate with $s_{\pm}$ symmetry.

We further calculate the mass enhancement parameter λ_{sf} due to spin fluctuations as a function of U. The result is shown in Fig. 9, where one can see that the mass enhancement raises rapidly once the system is tuned to the SDW instability. The same is seen in the dependence of the effective coupling constant $\lambda_{eff} = \lambda_{max}/(1 + \lambda_{sf})$, which is illustrated on the right scale of Fig. 9. λ_{eff} can reach pretty high values ≈ 0.7 as we vary U and the corresponding BCS $T_c = \omega_{sf} \exp(-1/\lambda_{eff}) \approx$ 139 K using $\omega_{sf} = 50$ meV. This estimate would, however,
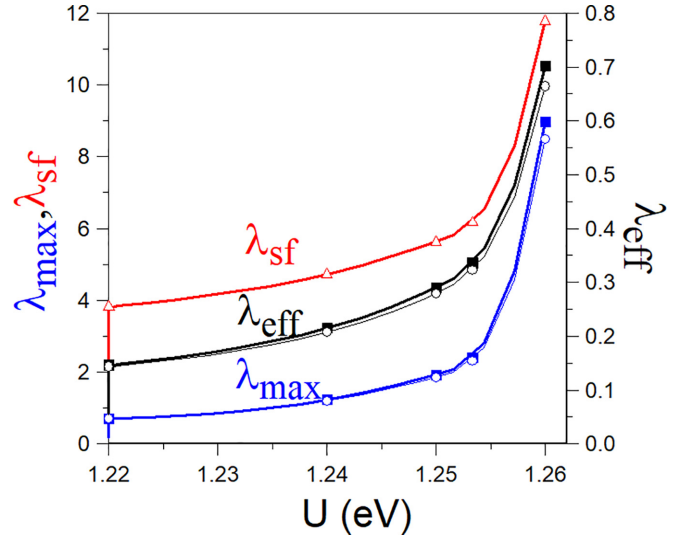

FIG. 9. Calculations using tight-binding parametrization of the LDA energy bands and the FLEX(RPA) method of the spin fluctuational mass enhancement, λ_{sf}, and of the two highest eigenvalues λ_{max} corresponding to $s_{\pm}$ (squares) and d_{xy} (circles) symmetries of the linearized BCS equation as a function of the on-site Hubbard interaction U for the two–orbital bilayer model of $La_3Ni_2O_7$. The effective coupling constant $\lambda_{eff} = \lambda_{max}/(1 + \lambda_{sf})$ is shown on the scale given on the right.

assume very large values of $\lambda_{sf} \approx 12$. More modest values of $\lambda_{sf} \approx 5$ correspond to $\lambda_{eff} \approx 0.3$, for which the BCS T_c is estimated to be about 20 K.

Clearly, one cannot expect the high accuracy from the RPA regarding the precise determination of the pairing interaction and the corresponding extraction of the T_c but one can judge that the inclusion of the full LDA-derived band structures lowers the estimate of the effective coupling constant as compared to the tight–binding calculation. This trend was also found by us in our recent exploration of the cuprate superconductor $HgBa_2CuO_4$ [41].

V. CONCLUSION

In conclusion, we used recently developed LDA + FLEX method to study the spin fluctuational mechanism of superconductivity in recently discovered $La_3Ni_2O_7$ under pressure. Based on this procedure, the superconducting scattering matrix elements between the Cooper pairs have been evaluated numerically, and the linearized BCS gap equation was exactly diagonalized. Our main result is the competition between d_{xy} and $s_{\pm}$ pairing symmetries for the most favorable eigenstate of the superconducting order parameter, which unfortunately cannot be precisely determined given the sensitivity of the result to the values of Hubbard parameter U used in the simulation. Since both symmetries can be distinguished by the presence or absence of nodes in the gap function, it should be straightforward to sort this out with currently on–going experiments.

The superconducting coupling constant λ_{max} as the highest eigenvalue of the BCS gap equations has been extracted together with the spin fluctuational mass enhancement

$m^*/m_{LDA} = 1 + \lambda_{sf}$. The effective coupling constant $\lambda_{eff} = \lambda_{max}/(1 + \lambda_{sf})$ was deduced as a function of U, but found to be modest and incapable to deliver high values of T_c unless U

is tuned to be close to SDW. We have also performed tight-binding calculations using a recently proposed two-orbital bilayer model which confirmed our conclusions.

---

[1] D. Li, K. Lee, B. Y. Wang, M. Osada, S. Crossley, H. R. Lee, Yi Cui, Y. Hikita, and H. Y. Hwang, Superconductivity in an infinite-layer nickelate, Nature (London) **572**, 624 (2019).

[2] H. Sun, M. Huo, X. Hu, J. Li, Z. Liu, Y. Han, L. Tang, Z. Mao, P. Yang, B. Wang, J. Cheng, D.–X. Yao, G.–M. Zhang, and M. Wang, Signatures of superconductivity near 80 K in a nickelate under high pressure, Nature (London) **621**, 493 (2023).

[3] J. Choisnet, R. A. Evarestov, I. I. Tupitsyn, and V. A. Veryazov, Investigation of the chemical bonding in nickel mixed oxides from electronic structure calculations, J. Phys. Chem. Solids **57**, 1839 (1996).

[4] M. J. Martínez-Lope, M. T. Casais, and J. A. Alonso, Stabilization of Ni+ in defect perovskites La(Ni$_{1-x}$Al$_x$)O$_{2+x}$ with 'infinite-layer' structure, J. Alloys Compd. **275-277**, 109 (1998).

[5] M. A. Hayward, M. A. Green, M. J. Rosseinsky, and J. Sloan, Sodium hydride as a powerful reducing agent for topotactic oxide deintercalation: Synthesis and characterization of the nickel(I) oxide LaNiO$_2$, J. Am. Chem. Soc. **121**, 8843 (1999).

[6] A. Ikeda, T. Manabe, and M. Naito, Improved conductivity of infinite-layer LaNiO$_2$ thin films by metal organic decomposition, Physica C **495**, 134 (2013).

[7] K.-W. Lee and W. E. Pickett, Infinite-layer LaNiO$_2$: Ni^{1+} is not Cu^{2+}, Phys. Rev. B **70**, 165109 (2004).

[8] V. I. Anisimov, D. Bukhvalov, and T. M. Rice, Electronic structure of possible nickelate analogs to the cuprates, Phys. Rev. B **59**, 7901 (1999).

[9] D. Li, B. Y. Wang, K. Lee, S. P. Harvey, M. Osada, B. H. Goodge, L. F. Kourkoutis, and H. Y. Hwang, Superconducting dome in Nd$_{1-x}$Sr$_x$NiO$_2$ infinite layer films, Phys. Rev. Lett. **125**, 027001 (2020).

[10] S. Zeng, C. S. Tang, X. Yin, C. Li, M. Li, Z. Huang, J. Hu, W. Liu, G. J. Omar, H. Jani, Z. S. Lim, K. Han, D. Wan, P. Yang, S. J. Pennycook, A. T. S. Wee, and A. Ariando, Phase diagram and superconducting dome of infinite-layer Nd$_{1-x}$Sr$_x$NiO$_2$ thin films, Phys. Rev. Lett. **125**, 147003 (2020).

[11] M. Osada, B. Y. Wang, B. H. Goodge, K. Lee, H. Yoon, K. Sakuma, D. Li, M. Miura, L. F. Kourkoutis, and H. Y. Hwang, A superconducting praseodymium nickelate with infinite layer structure, Nano Lett. **20**, 5735 (2020).

[12] For a review, see, e.g., C. C. Tsuei, and J. R. Kirtley, Pairing symmetry in cuprate superconductors, Rev. Mod. Phys. **72**, 969 (2000).

[13] For a review, see, e.g., D. J. Scalapino, A common thread: The pairing interaction for unconventional superconductors, Rev. Mod. Phys. **84**, 1383 (2012).

[14] For a review, see, e.g, P. A. Lee, N. Nagaosa, and X.-G. Wen, Doping a Mott insulator: Physics of high-temperature superconductivity, Rev. Mod. Phys. **78**, 17 (2006).

[15] For a review, see, e.g., *Theory of the Inhomogeneous Electron Gas*, edited by S. Lundqvist and S. H. March (Plenum, New York, 1983).

[16] V. Pardo and W. E. Pickett, Metal-insulator transition in layered nickelates La$_3$Ni$_2$O$_{7-\delta}$ (δ = 0.0, 0.5, 1), Phys. Rev. B **83**, 245128 (2011).

[17] X. Chen, P. Jiang, J. Li, Z. Zhong, and Y. Lu, Critical charge and spin instabilities in superconducting La$_3$Ni$_2$O$_7$, arXiv:2307.07154.

[18] V. Christiansson, F. Petocchi, and P. Werner, Correlated electronic structure of La$_3$Ni$_2$O$_7$ under pressure, Phys. Rev. Lett. **131**, 206501 (2023).

[19] D. A. Shilenko and I. V. Leonov, Correlated electronic structure, orbital-selective behavior, and magnetic correlations in double-layer La$_3$Ni$_2$O$_7$ under pressure, Phys. Rev. B **108**, 125105 (2023).

[20] F. Lechermann, J. Gondolf, S. Bötzel, and I. M. Eremin, Electronic correlations and superconducting instability in La$_3$Ni$_2$O$_7$ under high pressure, Phys. Rev. B **108**, L201121 (2023).

[21] For a review, see, e.g., G. Kotliar, S. Y. Savrasov, K. Haule, V. S. Oudovenko, O. Parcollet, and C. A. Marianetti, Electronic structure calculations with dynamical mean-field theory, Rev. Mod. Phys. **78**, 865 (2006).

[22] Z. Luo, X. Hu, M. Wang, W. Wu, and D.–X. Yao, Bilayer two-orbital model of La$_3$Ni$_2$O$_7$ under pressure, Phys. Rev. Lett. **131**, 126001 (2023).

[23] Y. Zhang, L.-F. Lin, A. Moreo, and E. Dagotto, Electronic structure, dimer physics, orbital-selective behavior, and magnetic tendencies in the bilayer nickelate superconductor La$_3$Ni$_2$O$_7$ under pressure, Phys. Rev. B **108**, L180510 (2023).

[24] W. Wu, Z. Luo, D.-X. Yao, and M. Wang, Charge transfer and Zhang-Rice singlet bands in the nickelate superconductor La$_3$Ni$_2$O$_7$ under pressure, arXiv:2307.05662.

[25] Y. Shen, M. Qin, and G.–M. Zhang, Effective bi-layer model Hamiltonian and density-matrix renormalization group study for the high-T_c superconductivity in La$_3$Ni$_2$O$_7$ under high pressure, Chin. Phys. Lett. **40**, 127401 (2023).

[26] Y. Gu, C. Le, Z. Yang, X. Wu, and J. Hu, Effective model and pairing tendency in bilayer Ni-based superconductor La$_3$Ni$_2$O$_7$, arXiv:2306.07275.

[27] Q. Qin and Y. F. Yang, High-T_c superconductivity by mobilizing local spin singlets and possible route to higher T_c in pressurized La$_3$Ni$_2$O$_7$, Phys. Rev. B **108**, L140504 (2023).

[28] Q.-G. Yang, D. Wang, and Q.-H. Wang, Possible $\mathcal{S}_\pm$-wave superconductivity in La$_3$Ni$_2$O$_7$, Phys. Rev. B **108**, L140505 (2023).

[29] Y.-H. Tian, Y. Chen, J.-M. Wang, R.-Q. He, and Z.-Y. Lu, Correlation effects and concomitant two-orbital -wave superconductivity in La$_3$Ni$_2$O$_7$ under high pressure, arXiv:2308.09698.

[30] Y. Zhang, L.-F. Lin, A. Moreo, T. A. Maier, and E. Dagotto, Structural phase transition, $\mathcal{S}_\pm$–wave pairing and magnetic stripe order in the bilayered nickelate superconductor La$_3$Ni$_2$O$_7$ under pressure, arXiv:2307.15276.

[31] Y.-B. Liu, J.-W. Mei, F. Ye, W.-Q. Chen, and F. Yang, $\mathcal{S} \pm -$ wave pairing and the destructive role of apical-oxygen deficiencies in La$_3$Ni$_2$O$_7$ under pressure, Phys. Rev. Lett. **131**, 236002 (2023).

[32] H. Liu, C. Xia, S. Zhou, and H. Chen, Role of crystal-field-splitting and long-range-hoppings on superconducting pairing symmetry of La$_3$Ni$_2$O$_7$, arXiv:2311.07316.

[33] D. J. Scalapino, E. Loh, Jr., and J. E. Hirsch, *d*–wave pairing near a spin-density-wave instability, Phys. Rev. B **34**, 8190 (1986).

[34] K. Miyake, S. Schmitt-Rink, and C. M. Varma, Spin-fluctuation-mediated even-parity pairing in heavy-fermion superconductors, Phys. Rev. B **34**, 6554 (1986).

[35] S. Doniach and S. Engelsberg, Low-temperature properties of nearly ferromagnetic fermi liquids, Phys. Rev. Lett. **17**, 750 (1966).

[36] N. F. Berk and J. R. Schrieffer, Effect of ferromagnetic spin correlations on superconductivity, Phys. Rev. Lett. **17**, 433 (1966).

[37] N. E. Bickers, D. J. Scalapino, and S. R. White, Conserving approximations for strongly correlated electron systems: Bethe-Salpeter equation and dynamics for the two-dimensional Hubbard model, Phys. Rev. Lett. **62**, 961 (1989).

[38] B. Menge and E. Miiller–Hartmann, The Hubbard model at high dimensions: Self-consistent weak coupling theory, Z. Phys. B **82**, 237 (1991).

[39] S. Y. Savrasov, G. Resta, and X. Wan, Local self-energies for V and Pd emergent from a nonlocal LDA+FLEX implementation, Phys. Rev. B **97**, 155128 (2018).

[40] V. I. Anisimov, F. Aryasetiawan, and A. I. Lichtenstein, First-principles calculations of the electronic structure and spectra of strongly correlated systems: The LDA+U method, J. Phys.: Condens. Matter **9**, 767 (1997).

[41] G. Heier, S. Y. Savrasov, Calculated spin fluctuational pairing interaction in HgBa$_2$CuO$_4$ using LDA+FLEX method, Phys. Rev. B **109**, 094506 (2024).

[42] For a review, see, e.g, D. J. Van Harlingen, Phase-sensitive tests of the symmetry of the pairing state in the high-temperature superconductors—Evidence for symmetry, Rev. Mod. Phys. **67**, 515 (1995).

[43] Z. Zhang, M. Greenblatt, and J. B. Goodenough, Synthesis, structure, and properties of the layered perovskite La$_3$Ni$_2$O$_{7-\delta}$, J. Solid State Chem. **108**, 402 (1994).

[44] S. Y. Savrasov, Linear-response theory and lattice dynamics: A muffin-tin-orbital approach, Phys. Rev. B **54**, 16470 (1996).

[45] E. Stenzel and H. Winter, The wave vector dependent dynamic spin susceptibilities of Pd and V and their contributions to the low temperature specific heat, J. Phys. F: Met. Phys. **16**, 1789 (1986).

[46] A. S. Alexandrov, Unconventional pairing symmetry of layered superconductors caused by acoustic phonons, Phys. Rev. B **77**, 094502 (2008).

[47] P. D. Johnson, T. Valla, A. V. Fedorov, Z. Yusof, B. O. Wells, Q. Li, A. R. Moodenbaugh, G. D. Gu, N. Koshizuka, C. Kendziora, Sha Jian, and D. G. Hinks, Doping and temperature dependence of the mass enhancement observed in the cuprate Bi$_2$Sr$_2$CaCu$_2$O$_{8+\delta}$, Phys. Rev. Lett. **87**, 177007 (2001).

[48] T. Valla, T. E. Kidd, W.-G. Yin, G. D. Gu, P. D. Johnson, Z.-H. Pan, and A. V. Fedorov, High-energy kink observed in the electron dispersion of high-temperature cuprate superconductors, Phys. Rev. Lett. **98**, 167003 (2007).

[49] B. P. Xie, K. Yang, D. W. Shen, J. F. Zhao, H. W. Ou, J. Weil, S. Y. Gu, M. Arita, S. Qiao, H. Namatame, M. Taniguchi, N. Kaneko, H. Eisaki, K. D. Tsuei, C. M. Cheng, I. Vobornik, J. Fujii, G. Rossi, Z. Q. Yang, and D. L. Feng, High-energy scale revival and giant kink in the dispersion of a cuprate superconductor, Phys. Rev. Lett. **98**, 147001 (2007).

[50] T. Dahm, V. Hinkov, S. V. Borisenko, A. A. Kordyuk, V. B. Zabolotnyy, J. Fink, B. Büchner, D. J. Scalapino, W. Hanke, and B. Keimer, Strength of the spin-fluctuation-mediated pairing interaction in a high-temperature superconductor, Nat. Phys. **5**, 217 (2009).

[51] N. Barišic, S. Badoux, M. K. Chan, C. Dorow, W. Tabis, B. Vignolle, G. Yu, J. Béard, X. Zhao, C. Proust, and M. Greven, Universal quantum oscillations in the underdoped cuprate superconductors, Nat. Phys. **9**, 761 (2013).

[52] For a review, see, e.g., M. Fujita, H. Hiraka, M. Matsuda, M. Matsuura, J. M. Tranquada, S. Wakimoto, G. Xu, and K. Yamada, Progress in neutron scattering studies of spin excitations in high-T_c cuprates, J. Phys. Soc. Jpn. **81**, 011007 (2012).

[53] H. A. Mook, M. Yethiraj, G. Aeppli, T. E. Mason, and T. Armstrong, Polarized neutron determination of the magnetic excitations in YBa$_2$Cu$_3$O$_7$, Phys. Rev. Lett. **70**, 3490 (1993).

[54] For a review, see, e.g., A. Damascelli, Z. Hussain, and Z.-X. Shen, Angle-resolved photoemission studies of the cuprate superconductors, Rev. Mod. Phys. **75**, 473 (2003).

[55] A. Lanzara, P. V. Bogdanov, X. J. Zhou, S. A. Kellar, D. L. Feng, E. D. Lu, T. Yoshida, H. Eisaki, A. Fujimori, K. Kishio, J.-I. Shimoyama, T. Noda, S. Uchida, Z. Hussain, and Z.-X. Shen, Evidence for ubiquitous strong electron–phonon coupling in high-temperature superconductors, Nature (London) **412**, 510 (2001).

[56] S. Y. Savrasov and O. K. Andersen, Linear-response calculation of the electron-phonon coupling in doped CaCuO$_2$, Phys. Rev. Lett. **77**, 4430 (1996).

[57] F. Giustino, M. L. Cohen, and S. G. Louie, Small phonon contribution to the photoemission kink in the copper oxide superconductors, Nature (London) **452**, 975 (2008).

[58] R. Coldea, S. M. Hayden, G. Aeppli, T. G. Perring, C. D. Frost, T. E. Mason, S.-W. Cheong, and Z. Fisk, Spin waves and electronic interactions in La$_2$CuO$_4$, Phys. Rev. Lett. **86**, 5377 (2001).